nature nanotechnology

LETTERS

PUBLISHED ONLINE: 4 AUGUST 2013 | DOI: 10.1038/NNANO.2013.143

Realization of pristine and locally tunable one-dimensional electron systems in carbon nanotubes

J. Waissman[1,2†], M. Honig[1†], S. Pecker[1†], A. Benyamini[1†], A. Hamo[1†] and S. Ilani[1*]

The ability to tune local parameters of quantum Hamiltonians has been demonstrated in experimental systems including ultracold atoms[1], trapped ions[2], superconducting circuits[3] and photonic crystals[4]. Such systems possess negligible disorder, enabling local tunability. Conversely, in condensed-matter systems, electrons are subject to disorder, which often destroys delicate correlated phases and precludes local tunability. The realization of a disorder-free and locally-tunable condensed-matter system thus remains an outstanding challenge. Here, we demonstrate a new technique for deterministic creation of locally-tunable, ultralow-disorder electron systems in carbon nanotubes suspended over complex electronic circuits. Using transport experiments we show that electrons can be localized at any position along the nanotube and that the confinement potential can be smoothly moved from location to location. The high mirror symmetry of transport characteristics about the nanotube centre establishes the negligible effects of electronic disorder, thus allowing experiments in precision-engineered one-dimensional potentials. We further demonstrate the ability to position multiple nanotubes at chosen separations, generalizing these devices to coupled one-dimensional systems. These capabilities could enable many novel experiments on electronics, mechanics and spins in one dimension.

The carbon nanotube is a promising substrate for realizing an ultraclean and locally tunable electron system. In contrast to conventional semiconductors, carbon nanotubes have been shown to grow exceptionally cleanly, leading to low inherent disorder[5]. Moreover, the long lengths of this one-dimensional system suggest the possibility of controlling the potential at each point along its length using an array of transverse electrostatic gates (Fig. 1a). Nanotubes also demonstrate a range of desirable physical properties[6]. For example, their strong electron–electron interactions could generate correlated electronic ground states[7–10], the ability to localize and control individual spins could realize a quantum information chain or charge/spin pumps[11–17], and these degrees of freedom can interact with its mechanical motion[18–21] or with correlated materials[22–26].

To date, studies have mainly exploited these properties in zero-dimensional single and double quantum dot settings. The extension to longer one-dimensional settings has so far been hindered by disorder, which at low temperatures breaks the electron system into localized, uncontrolled quantum dots[27,28]. The bottleneck lies in the conventional technologies used for making ultraclean nanotube devices, which require two demanding processes to succeed simultaneously: the growth of pristine nanotubes and the fabrication of complex electrical circuits. Nanotube cleanliness is achieved by growing the nanotubes as the last step in device fabrication[5], but this limits the device materials and design because of the high temperature required for nanotube growth. Recent stamping approaches[17,29] have eliminated some of these issues by growing nanotubes separately from the measurement circuit and transferring them mechanically. However, these approaches remain statistical in nature, resulting in a small yield of a few percent even for simple and short devices. Increasing the device complexity with either longer nanotube's or more complex circuits will decrease the yield further, rendering these approaches less practical. Thus, the potential of the nanotube as a system for locally tunable experiments in extended one-dimensional geometries remains unrealized.

In this Letter we report the realization of a new nanoassembly technique that allows us to deterministically create ultralow-disorder, suspended, multinanotube devices with electrical circuits of arbitrary complexity. Our approach uses scanning probe microscope manipulation to achieve deterministic assembly. On one chip we grow long, parallel nanotubes suspended without slack over wide trenches (Fig. 1b; see Methods). On a separate chip we fabricate the electrical circuit on a narrow cantilever (Fig. 1c). For the device in Fig. 1a, for example, an array of parallel electrodes is fabricated, where the outer ones (contacts, yellow) are taller than the rest (gates, blue). The nanotubes and circuits are fabricated using two independent processes, and neither imposes any restrictions on the other. The scanning probe microscope is then used to insert the cantilever into a trench and 'mate' it with a nanotube (Fig. 1d). Because the contacts are taller than the gates, the nanotube touches them first and remains suspended over the gates (Fig. 1e). Importantly, this process works at low temperatures ($T = 4$ K), where electronic cleanliness can be tested via *in situ* transport measurements. By mating to nanotubes in different trenches, or to different segments of one nanotube, we can therefore select only perfectly clean tubes, with chosen bandgaps, and assemble them into complex devices in a deterministic way.

To find the desired nanotube we must browse through several trenches, connecting and detaching from different nanotubes without crashing or contaminating the cantilever. To do this safely without visual aids we implemented a capacitance-based detection scheme (see Methods) that, together with piezoelectric positioners, allows control of the relative positions of the two chips with ~1 μm accuracy. The final approach is done by a piezoelectric scanner with nanometre accuracy, allowing the cantilever to gently touch the tube at any depth inside the trench, and to finely control the nanotubes lateral position along the circuit. Contact to a nanotube is identified by a change in resistance between the two chips, and the circuit is lowered until the nanotube touches all contact electrodes. At this point, we measure *in situ* gate-dependent

[1]Department of Condensed Matter Physics, Weizmann Institute of Science, Rehovot 76100, Israel, [2]School of Engineering and Applied Sciences, Harvard University, Cambridge, Massachusetts 02138, USA; †These authors contributed equally to this work. *e-mail: shahal.ilani@weizmann.ac.il

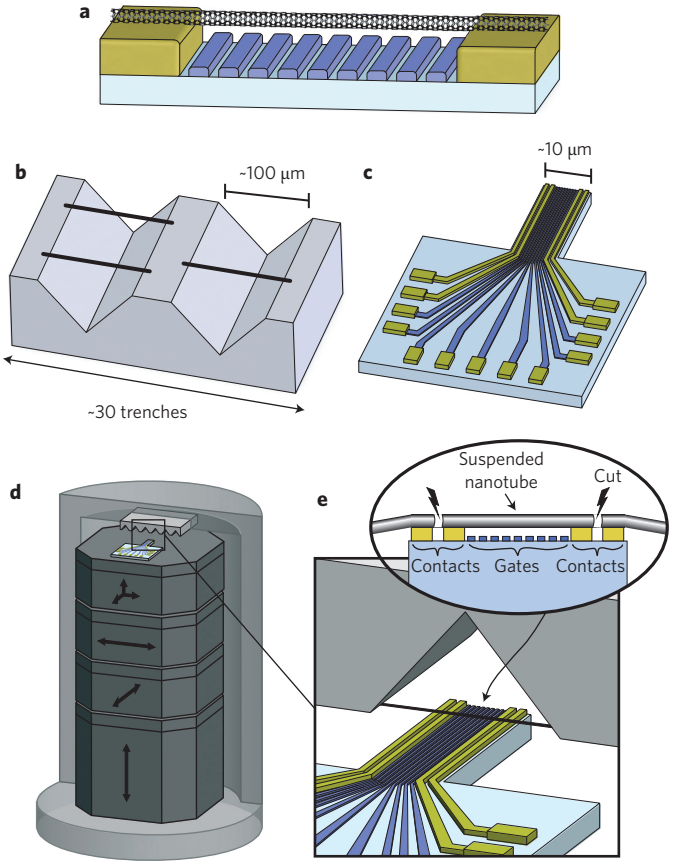

Figure 1 | Illustration of the nanoassembly technique for creating clean and complex nanotube devices. a, Example of a device with desirable characteristics: a nanotube connected to source and drain electrodes (yellow) and suspended above multiple gates (blue). **b**,**c**, We assemble such a device from two independent chips: the 'nanotube chip' with parallel nanotubes grown over wide trenches (**b**) and the 'circuit chip' consisting of contact electrodes (yellow) and gate electrodes (blue) formed on a narrow cantilever (**c**). Typical dimensions are indicated. **d**, The nanoassembly is achieved with a scanning probe microscope (illustrated), which controls the relative position of the two chips with high precision (arrows indicate directions of motion). **e**, A device is made by inserting the cantilever into a trench and 'mating' the electrical circuit to several nanotubes until a desirable one is found. The nanotube touches the taller metallic contacts and remains suspended over the gates, allowing *in situ* transport measurements (inset). Once a desirable nanotube is identified, it is locally cut by passing a large current between adjacent pairs of side contacts, without damaging the suspended segment (Supplementary Section S1), disconnecting the device from the nanotube chip.

transport. Having identified a desirable nanotube, we pass high current through adjacent pairs of contacts at the sides of the device to surgically cut the nanotube at well-defined locations and separate it from the nanotube chip without damaging the segment above the gates (Fig. 1e; Supplementary Section S1).

Figure 2c presents a representative seven-gate device made using our mating technique with nanotube and circuit chips similar to those shown in Fig. 2a,b. The nanotube is perpendicular to the gates, is suspended without slack over a length of 1.2 μm at a fixed height of 130 nm above all gates, is anchored over the entire length of the contacts, and does not touch the silicon oxide. These characteristics are achieved in the vast majority of mated devices (Supplementary Section S2). To localize multiple nanotubes at specific locations, we pattern contacts of different lengths and move the cantilever along the trench with the piezo-scanner,

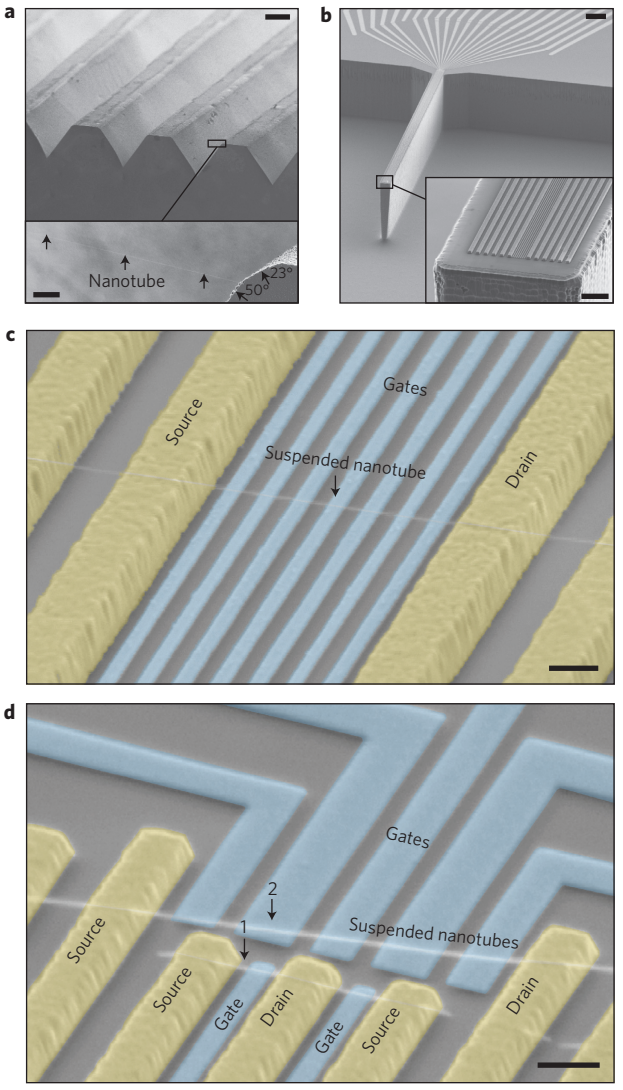

Figure 2 | Individual components of the mating technique and representative nanoassembled devices. a, Top: scanning electron microscope (SEM) image of the 'nanotube chip' comprising 30 trenches, ~100 μm wide, etched in a silicon wafer and metallized with platinum. Suspended nanotubes are grown from the plateaux between trenches (see Methods). Scale bar, 50 μm. Bottom: zoom-in on a trench edge showing a single nanotube growing across the trench. The nanotube growth direction is aligned perpendicular to the trenches by the feedstock gas flow. A shallow slope at the trench edge (see Methods) allows the nanotubes to stick easily to the surface, removing their slack (angles of the two slopes are indicated; scale bar, 4 μm). **b**, SEM image of the 'circuit chip', patterned on a Si/SiO_2 wafer, with 155-nm-high gold contacts and 25-nm-high PdAu gates. Deep etching leaves these electrodes on a thin (~10 μm) and tall (~100 μm) cantilever. Scale bar, 20 μm. Inset: zoom-in to the cantilever tip. Scale bar, 2 μm. **c**, A nanoassembled device with a single nanotube connected to contacts (yellow) and suspended at a height of 130 nm over seven gates (blue, 150 nm pitch). Scale bar, 200 nm. **d**, A two-nanotube device: the first nanotube sits on three contacts with two matching gates. The second nanotube is suspended over five gates, which wrap around its contacts for independent addressability. Here, the shortest nanotube–nanotube distance is ~300 nm, and the accuracy of positioning the nanotube from the opposite contact edge is less than 85 nm. After mating, the nanotubes were selectively cut at two adjacent contact pairs (visible, for example, for nanotube 1; Supplementary Section S1), isolating the two devices from one another. Scale bar, 300 nm. (Supplementary Section S8 shows measurements for this device.)

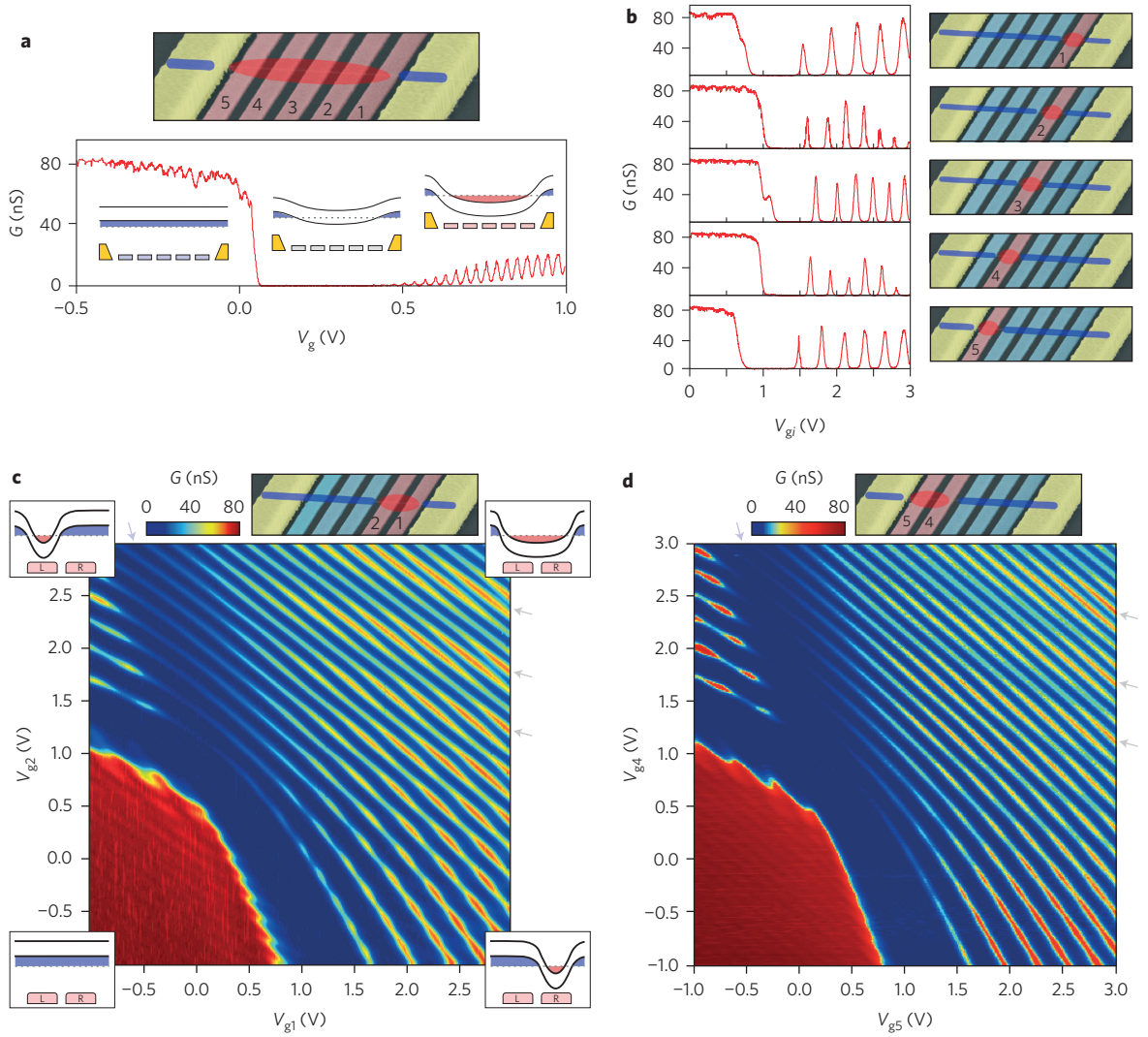

Figure 3 | Localizing and moving electrons in clean quantum dots on a five-gated, small-bandgap nanotube device. a, Top: SEM image of a device similar to the one measured (gate numbers are indicated). The nanotube is locally coloured according to its doping: holes, blue; electrons, red. The suspended segment is electrostatically doped by the gates, whereas the segments above the contacts are hole-doped by the metal. Bottom: conductance G measured as a function of a common voltage on all five gates, V_g. Coulomb oscillations are apparent at positive gate voltages due to the formation of a quantum dot extended over the entire suspended nanotube. Insets: position-dependent nanotube band diagrams in the three different conductance regimes: a hole-doped 'nanotube wire', the nanotube bandgap and electron Coulomb oscillations (hole band, blue; electron band, red). **b**, Similar measurements to **a** as a function of voltages on five individual gates, V_{gi} (where i is the gate index), while the other gates maintain a fixed hole-doping voltage, $V_{gj} = -0.8$ V, $j \neq i$. In each trace a small electron quantum dot is formed above the corresponding gate (side illustrations). **c**, Conductance G (colour map), measured as a function of the voltages on two adjacent gates, V_{g1} and V_{g2} (top illustration). Corner overlays show schematic band diagrams for different applied voltages. From the bottom-right to top-left corner, a dot is continuously shifted between the two adjacent gates. **d**, Similar measurement to **c** for the mirror-symmetric experiment with gates 4 and 5. Although the values of conductance differ between **c** and **d** due to different p–n junction barriers formed near the left and right contacts, the conductance patterns are remarkably similar, down to small details (see main text).

successively touching and detaching from a tube until resistance measurements indicate that it is touching contacts corresponding to a specific location. Figure 2d shows a double-nanotube device made with this technique. The first nanotube is positioned on a set of shorter contacts, with matching gates, and cut to electrically isolate it from all other contacts. The second nanotube is then positioned on a longer set of contacts, with a second set of gates wrapped around the longer contacts, allowing both nanotubes to be independently contacted and gated (Supplementary Section S8 shows measurements demonstrating electrostatic coupling of the two nanotubes). Geometrically, the device in Fig. 2c is the closest yet achieved to the ideal illustrated in Fig. 1a, and the device in Fig. 2d extends this capability to a new class of devices with multinanotube geometry.

Are these devices as ideal electronically as they are geometrically? We address this question using transport measurements of multiply-gated devices with small-bandgap nanotubes. We start with the simplest experiment on a five-gated device, with all gates chained together, reproducing past single-gate transistor experiments. We use gold contacts that dope the nanotube segments above them with holes, and control the doping of the suspended nanotube segment electrostatically with the gates. As a function of the gate voltage the conductance measured at $T = 4$ K shows three regimes (Fig. 3a). At negative voltages the suspended segment is hole-doped, forming a continuous 'nanotube wire', the conductance of which is weakly gate-dependent[27]. At intermediate voltages the nanotube is doped into its bandgap, determined to be 34 ± 5 meV from finite bias measurements, and the conductance is suppressed.

For positive voltages the suspended segment is doped with electrons, forming a pair of p–n junctions near the contacts that confine a large quantum dot, whose charging by individual electrons generates Coulomb blockade oscillations in the conductance. The oscillation periodicity $\Delta V_g = 31.5 \pm 1.5$ mV, given by $\Delta V_g = e/C_g$ (where e is the electron charge and C_g is the gate capacitance), agrees well with that expected from the capacitance of the length of the suspended segment, $L = 880$ nm, to all five gates. The corresponding charging energy of this large dot, obtained from finite-bias Coulomb diamonds, is $E_C = 10 \pm 2$ meV. The clean and regular spectrum of oscillations therefore signifies the formation of a single quantum dot over the entire suspended nanotube length, the electronic cleanliness of which is comparable to the best ultra-clean nanotube devices made to date[5,9,12,30].

The local gates now allow us to probe electronic behaviour on finer spatial scales. By electron-doping the nanotube locally with a single gate, and hole-doping the rest of it with all other gates, we form a smaller quantum dot localized above this gate. Accordingly, with five independent gates we can form, in principle, dots at five different locations along the nanotube, the characteristics of which reflect the spatial dependence of the nanotube electronic properties. Figure 3b shows the corresponding five conductance traces as a function of the individual gate voltages. Clearly, single quantum dots are formed at all positions. Their Coulomb blockade oscillations have periodicities of $\Delta V_g = 280 \pm 10$ mV, indicating that the dots are well localized above a single gate (Supplementary Section S4). The corresponding charging energy of these dots is $E_C = 59 \pm 8$ meV. Moreover, all traces exhibit a single periodicity, showing that the dots are clean. The Coulomb peak heights, however, vary between dots at different locations, hinting at possible position-dependence in the electronic properties along the nanotube.

A more complete picture of the spatial dependence is obtained by using pairs of gates to continuously move a quantum dot along the nanotube. Figure 3c shows the conductance measured as a function of the voltages on gates 1 and 2, while all other gates are negatively biased. At the bottom left corner, both gates dope the nanotube with holes and no dot is formed. When gate 1 (gate 2) is positively biased, along the horizontal (vertical) axis, a dot forms above this gate. Biasing both gates together (upper-right corner) extends the dot above both gates. Thus, going from the bottom right to the top left of Fig. 3c, the quantum dot shifts from one gate to its neighbour. In this measurement, the Coulomb charging peaks appear as charging lines, separating different charge states of the quantum dot. Their local slope corresponds to the relative capacitance of the dot to the two gates, and reflects the position of the centre-of-mass of the electronic charge. Notably, the slopes of all charging lines, down to that of the first electron, evolve smoothly and monotonically during the shift, reflecting the smooth transfer of the electronic confinement from site to site. The data, however, contain unexpected features: the charging lines exhibit periodic stripe modulation of the peak heights and a band-like region where the conductance is suppressed (Fig. 3c, arrows). These features may indicate the existence of disorder that forms random barriers or dots. In the following we show, however, that these features arise from intrinsic electrostatics, and not disorder.

A clear way to determine whether the observed features are due to disorder is to perform the mirror-symmetric version of the experiment depicted in Fig. 3c. This measurement, shown in Fig. 3d, is done with the opposite gates, 4 and 5, over a voltage range identical to that in Fig 3c. Comparing these mirror-symmetric measurements reveals a striking similarity: charging line slopes, positions and spacing are all identical. Furthermore, the peak modulations and conductance suppression are reproduced at the same gate voltages. The remarkable implication is that all the observed features are not the result of a random disorder potential, but instead arise from the intrinsic electrostatics of the device. These features, discussed further in Supplementary Section S5, are due to gating of nanotube segments that are beyond the dot, such as Fabry–Perot-like oscillations in the hole-doped 'nanotube leads'. In contrast to peak positions, which are identical in both experiments, the peak heights differ. Although the peak positions are sensitive only to electrostatics, their heights also depend on the resistance to the metal contacts, which might vary for different contacts. We find, however, that this asymmetry does not originate in contact resistance but is, instead, also electrostatic in nature, arising from an inequivalence of the p–n junction barriers near the source and drain contacts due to a slight lithographic misalignment (~15 nm) of the gates towards the drain contact. The observation of nearly perfect mirror symmetry thus demonstrates that, for electrons above the outer gates, electrostatics rather than random disorder determines the local electronic structure.

To check the effects of disorder in the bulk of the suspended nanotube, we generalize the above measurements to all pairs of gates in the device. Figure 4 shows a matrix of two-gate conductance measurements, the columns and rows of which correspond to the gates scanned on the horizontal and vertical axes of each panel. In all panels the gate voltage ranges are identical, with all other gates maintaining a constant hole-doping voltage. On the main diagonal of this matrix, the scanned gates are nearest neighbours (as in Fig. 3c,d). Clearly, all the scans along this diagonal feature a continuous bending of the charging lines, indicating the smooth movement of charge from any gate to its neighbour. Scans with non-adjacent gates form two or more quantum dots along the nanotube. Many features are observed in these experiments, but the remarkable observation is that over the entire matrix all these features are symmetric among experiments with mirror symmetry around the nanotube centre (dashed black line). We conclude that, to the spatial resolution fixed by our gates and to the energy scale set by the temperature, disorder is playing a negligible role in determining the potential landscape along the entire device. Measurements on a different device show similar device cleanliness down to dilution refrigerator temperatures (Supplementary Section S7).

The last step to establish our system as a controllable laboratory for one-dimensional experiments is to demonstrate a quantitative understanding of its electrostatics, allowing the design of one-dimensional potentials. A potential can be defined if the gates are placed close to the suspended nanotube compared to their pitch. Close gates, however, screen electron–electron interactions, inhibiting this highly desirable feature. It is therefore beneficial to distance the gates from the nanotube, but this results in non-local gating, and accurate design of the potential requires a quantitative accounting of this non-locality. This information, how a gate at position i influences the nanotube at a position above gate j, is embedded in Fig. 4. At the bottom right corner of each (i,j) panel a quantum dot is localized over gate i and gated by gate j. The dot, acting as a local charge detector, allows us to directly measure the capacitive coupling elements C_{ij} (25 in total; see Supplementary Section S3 for details). The inset of Fig. 4 presents the extracted capacitance distribution for each gate (points), and compares it with calculated capacitance distributions from a finite-element simulation (lines). These calculations, with no free parameters, fit the experimental points quantitatively well. Specifically, we see that the capacitance distributions of gates 2–4 are almost identical, demonstrating that the electrostatics in the bulk of the sample is translationally invariant. The edge gates (1 and 5) show reduced coupling due to screening by the contacts, and differ in their peak coupling due to the gate-contact misalignment asymmetry noted above, fully reproduced by the calculations. These results are not sensitive to mechanical displacement of the nanotube, which for this device with 1 V applied to all five gates is estimated to be ~5 nm, small compared to the 130 nm gate–nanotube distance. Using these calculations, we put an upper bound of $\sim 5 \times 10^{-2} e$ on the level of charge disorder on 100 nm

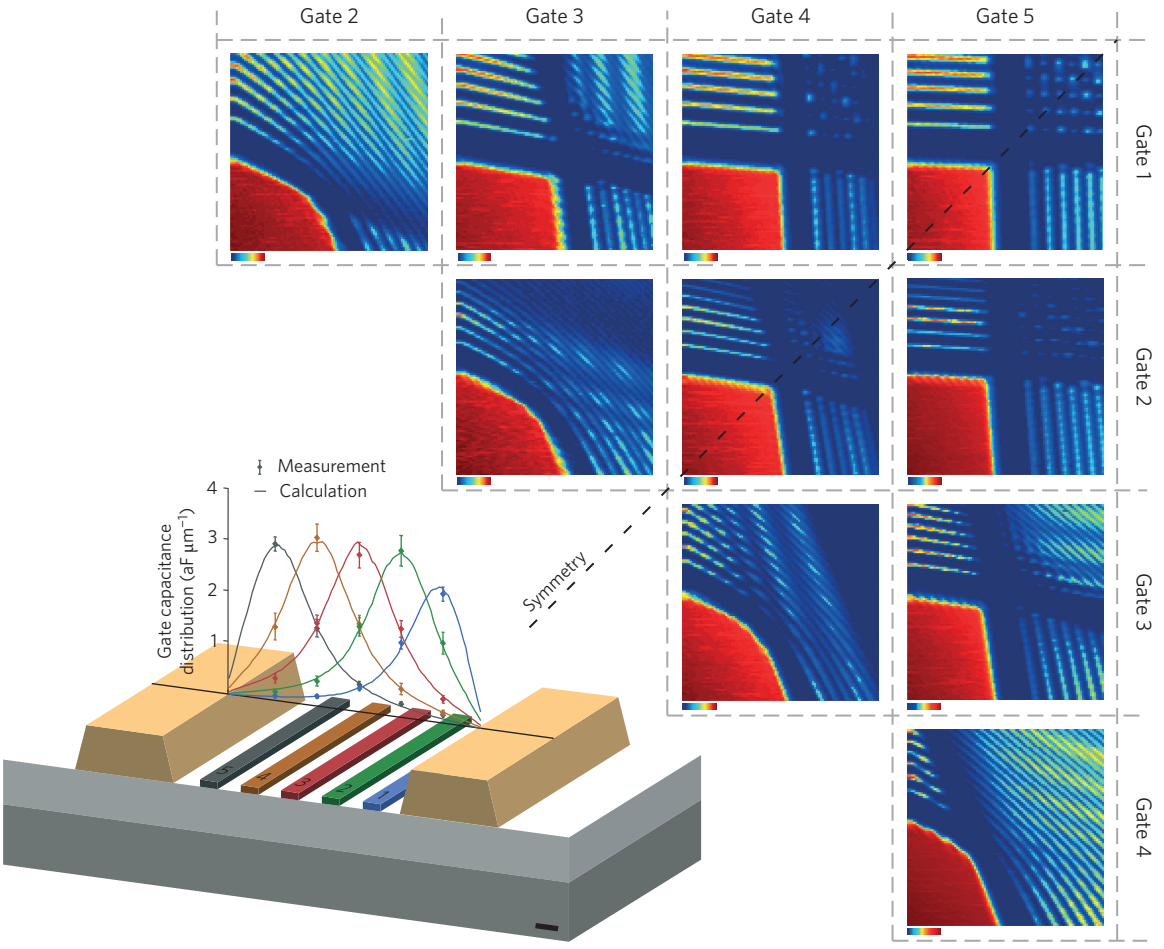

Figure 4 | Characterization of the disorder and local electrostatic environment of the nanotube. Main panel: a matrix of conductance measurements. In each entry a different pair of gate voltages, V_{gi} and V_{gj}, is scanned. The gate scanned along the horizontal (vertical) axis is indicated in the column (row) title, and the voltage scan range in all panels is identical to that in Fig. 3c,d. The detailed conductance features in all panels show symmetry with respect to mirror reflection around the nanotube centre (dashed black line). Colour maps for all measurements are shown in the lower left corner of each entry, over the range 0–80 nS for all scans. Inset: electrostatic coupling between individual gates and the nanotube. Same-colour points show the extracted capacitive coupling between a given gate and five different quantum dots formed along the nanotube. Corresponding lines show the capacitance distribution of the gate to the nanotube calculated with a finite-element simulation incorporating the full device geometry, including the gate–contact misalignment of ~15 nm (Supplementary Section S3). Without any free parameters, the two show excellent agreement.

length scales, corresponding to ~5 mV of bare disorder potential or ~50 μV in the self-consistent disorder potential (Supplementary Section S4). These low values of disorder and the correspondence of the measured and calculated electrostatics show that potential profiles can be accurately designed. In Supplementary Section S6, we show how detailed knowledge of the capacitive coupling elements C_{ij} allows us to deconvolve the effect of the nanotube–gate separation and design potentials with resolution limited only by the density of gates.

The ability to identify ultraclean nanotubes and selectively nanoassemble them at predefined positions in an electronic circuit allows the fabrication of novel devices. The assembly of electronically pristine 1–2-μm-long multigated devices is performed in a few hours, suggesting that even more complex devices can be fabricated with this technique. These devices constitute a system for studying the electronic phases of strongly interacting electrons in one dimension, subject to engineered potentials. They could also act as clean mechanical resonators that can be coupled to multiple quantum dots. Furthermore, we have demonstrated devices involving multiple nanotubes positioned at chosen locations, heralding sensitive local charge detectors and coupled one-dimensional systems (Supplementary Section S8). We expect these novel devices to lead to new experiments in nanotubes with applications ranging from fundamental condensed-matter physics to nanoelectromechanics and quantum information science.

Methods

The 'nanotube chip' was formed in a two-step etching process. The first etch, in KOH solution, formed deep, wide trenches with ~50° wall angles, while the second etch, in tetramethylammonium hydroxide (TMAH) solution, formed a shallow trench lip with an ~23° angle (Fig. 2a, inset). This shallow lip allows nanotubes to easily stick to the surface after growth, which eliminates their slack. The chip was then metallized with Ti/Pt (5 nm/150 nm, respectively). Nanotubes were grown from catalyst deposited on the plateaux between trenches in lithographically defined pads. Growth was performed with chemical vapour deposition using a standard growth recipe for single-walled carbon nanotubes, with argon, hydrogen and ethylene gases. Feedstock gas flow alignment ensured the growth of parallel suspended nanotubes (±3°).

The 'circuit chip' was patterned on a Si/SiO_2 wafer using electron-beam lithography, followed by the evaporation of contacts (5 nm/150 nm Ti/Au), gates (5 nm/20 nm Ti/PdAu) and deep reactive ion etching with lithographically defined etch masks.

We found that an important step for establishing good electrical and mechanical contact between a nanotube and contact electrodes lies in the *in situ* cleaning of the contact surfaces using argon ion etching in a load-lock. Immediately after this etching, the sample was inserted into the microscope for mating. With this step, we achieved mechanically stable contacts with typical resistances of ~100 kΩ measured

at room temperature. These values are typical for these kinds of devices, although still falling short of the resistances demonstrated[31] in some devices that approach $R = h/4e^2$.

Blind navigation in the microscope was performed with capacitance measurements. Four metal pads were patterned on the measurement circuit chip, two large pads of area ~75,000 μm^2 each and two small pads of ~5,000 μm^2 each. Their capacitance was measured with respect to the metallized nanotube chip, which served as the second electrode. The pads were designed such that scanning allowed us to establish, with rough and fine resolution, the relative position and angle of the two chips. The capacitance was measured using a displacement current at a frequency of ~12 kHz as a function of nano-positioner movement (Attocube). The separation between the two chips and the orientation and relative position of their edges were first determined. A final scan with a small capacitor parallel to the trenches established the trench positions for mating. Overall, we determined the relative position and orientation of the two chips in all three dimensions to within ~1 μm and ~0.1°, respectively.

Conductance measurements were performed with standard a.c. lock-in techniques, using 100 μV excitation.

Received 10 January 2013; accepted 19 June 2013; published online 4 August 2013

References

1. Bloch, I., Dalibard, J. & Nascimbène, S. Quantum simulations with ultracold quantum gases. *Nature Phys.* **8,** 267–276 (2012).
2. Blatt, R. & Roos, C. F. Quantum simulations with trapped ions. *Nature Phys.* **8,** 277–284 (2012).
3. Houck, A. A., Türeci, H. E. & Koch, J. On-chip quantum simulation with superconducting circuits. *Nature Phys.* **8,** 292–299 (2012).
4. Aspuru-Guzik, A. & Walther, P. Photonic quantum simulators. *Nature Phys.* **8,** 285–291 (2012).
5. Cao, J., Wang, Q. & Dai, H. Electron transport in very clean, as-grown suspended carbon nanotubes. *Nature Mater.* **4,** 745–749 (2005).
6. Jorio, A., Dresselhaus, G. & Dresselhaus, M. S. (eds) in *Carbon Nanotubes: Advanced Topics in the Synthesis, Structure, Properties and Applications* 455–493 (Springer, 2008).
7. Yao, Z., Postma, H. W. C., Balents, L. & Dekker, C. Carbon nanotube intramolecular junctions. *Nature* **402,** 273–276 (1999).
8. Bockrath, M. *et al.* Luttinger-liquid behaviour in carbon nanotubes. *Nature* **397,** 598–601 (1999).
9. Deshpande, V. V. & Bockrath, M. The one-dimensional Wigner crystal in carbon nanotubes. *Nature Phys.* **4,** 314–318 (2008).
10. Deshpande, V. V. *et al.* Mott insulating state in ultraclean carbon nanotubes. *Science* **323,** 106–110 (2009).
11. Loss, D. & DiVincenzo, D. P. Quantum computation with quantum dots. *Phys. Rev. A* **57,** 120–126 (1998).
12. Kuemmeth, F., Ilani, S., Ralph, D. C. & McEuen, P. L. Coupling of spin and orbital motion of electrons in carbon nanotubes. *Nature* **452,** 448–452 (2008).
13. Buitelaar, M. *et al.* Adiabatic charge pumping in carbon nanotube quantum dots. *Phys. Rev. Lett.* **101,** 126803 (2008).
14. Churchill, H. *et al.* Relaxation and dephasing in a two-electron ^{13}C nanotube double quantum dot. *Phys. Rev. Lett.* **102,** 2–5 (2009).
15. Kuemmeth, F., Churchill, H. O. H., Herring, P. K. & Marcus, C. M. Carbon nanotubes for coherent spintronics. *Mater. Today* **13,** 18–26 (2010).
16. Jespersen, T. S. *et al.* Gate-dependent spin–orbit coupling in multielectron carbon nanotubes. *Nature Phys.* **7,** 348–353 (2011).
17. Pei, F., Laird, E. A., Steele, G. A. & Kouwenhoven, L. P. Valley–spin blockade and spin resonance in carbon nanotubes. *Nature Nanotech.* **7,** 630–634 (2012).
18. Sazonova, V. *et al.* A tunable carbon nanotube electromechanical oscillator. *Nature* **431,** 284–287 (2004).
19. Leturcq, R. *et al.* Franck–Condon blockade in suspended carbon nanotube quantum dots. *Nature Phys.* **5,** 327–331 (2009).
20. Steele, G. A. *et al.* Strong coupling between single-electron tunneling and nanomechanical motion. *Science* **325,** 1103–1107 (2009).
21. Lassagne, B. *et al.* Coupling mechanics to charge transport in carbon nanotube mechanical resonators. *Science* **325,** 1107–1110 (2009).
22. Sahoo, S. *et al.* Electric field control of spin transport. *Nature Phys.* **1,** 99–102 (2005).
23. Jarillo-Herrero, P., Van Dam, J. A. & Kouwenhoven, L. P. Quantum supercurrent transistors in carbon nanotubes. *Nature* **439,** 953–956 (2006).
24. Hauptmann, J. R., Paaske, J. & Lindelof, P. E. Electric-field-controlled spin reversal in a quantum dot with ferromagnetic contacts. *Nature Phys.* **4,** 373–376 (2008).
25. Pillet, J-D. *et al.* Andreev bound states in supercurrent-carrying carbon nanotubes revealed. *Nature Phys.* **6,** 965–969 (2010).
26. Schindele, J., Baumgartner, A. & Schönenberger, C. Near-unity Cooper pair splitting efficiency. *Phys. Rev. Lett.* **109,** 157002 (2012).
27. McEuen, P., Bockrath, M., Cobden, D., Yoon, Y-G. & Louie, S. Disorder, pseudospins, and backscattering in carbon nanotubes. *Phys. Rev. Lett.* **83,** 5098–5101 (1999).
28. Woodside, M. T. & McEuen, P. L. Scanned probe imaging of single-electron charge states in nanotube quantum dots. *Science* **296,** 1098–1101 (2002).
29. Wu, C. C., Liu, C. H. & Zhong, Z. One-step direct transfer of pristine single-walled carbon nanotubes for functional nanoelectronics. *Nano Lett.* **10,** 1032–1036 (2010).
30. Steele, G. A., Gotz, G. & Kouwenhoven, L. P. Tunable few-electron double quantum dots and Klein tunnelling in ultraclean carbon nanotubes. *Nature Nanotech.* **4,** 363–367 (2009).
31. Liang, W. *et al.* Fabry–Perot interference in a nanotube electron waveguide. *Nature* **411,** 665–669 (2001).

Acknowledgements

The authors thank N. Shadmi and E. Joselevich for nanotube growth in the initial stages of the project, D. Mahalu for electron-beam writing, A. Yoffe and S. Garusi for dry etching and F. Kuemmeth, P. McEuen, H. Shtrikman, F. von-Oppen and A. Yacoby for comments on the manuscript. S.I. acknowledges financial support from the ISF Legacy Heritage foundation (grant 2005/08-80.0), the Bi-National Science Foundation (BSF) (grant 710647-03), the Minerva Foundation (grant 780054), the ERC Starters (grant 258753), the Marie Curie People (grant 239322) (IRG) and the Alon Fellowship. S.I. is incumbent of the William Z. and Eda Bess Novick career development chair.

Author contributions

All authors conceived, designed and performed the experiments. J.W., S.P., A.B., A.H. and S.I. analysed the data. S.P., A.B. and A.H. contributed analysis tools. J.W. and S.I. wrote the paper.

Additional information

Supplementary information is available in the online version of the paper. Reprints and permissions information is available online at www.nature.com/reprints. Correspondence and requests for materials should be addressed to S.I.

Competing financial interests

The authors declare no competing financial interests.